Electronic Supplementary Material (ESI) for Physical Chemistry Chemical Physics.
This journal is © the Owner Societies 2022

Electronic supporting information for

Triplet-triplet sensitizing within pyrene-based *COO*-BODIPY: A breaking molecular platform for annihilating photon upconversion

Christopher Schad,[a] Edurne Avellanal-Zaballa,[b] Esther Rebollar,[c] César Ray,[a] Eduardo Duque-Redondo,[b] Florencio Moreno,[a] Beatriz L. Maroto,[a] Jorge Bañuelos,*[b] Inmaculada García-Moreno,*[c] and Santiago de la Moya*[a]

[a] *Depto. de Química Orgánica I, Facultad de CC. Químicas, Universidad Complutense de Madrid, Ciudad Universitaria s/n, 28040, Madrid, Spain. E-mail: santmoya@ucm.es*

[b] *Depto. de Química Física, Universidad del Pais Vasco-EHU, Apartado 644, 48080, Bilbao, Spain. E-mail: jorge.banuelos@ehu.es*

[c] *Depto. de Química-Física de Materiales, Instituto de Química-Física Rocasolano, Centro Superior de Investigaciones Científicas (CSIC), Serrano 119, 28006 Madrid, Spain. E-mail: i.garcia-moreno@iqfr.csic.es*

Table of contents

1. General methods, instrumentation and techniques

Synthesis

All reagents were used without purification. All solvents were of HPLC grade and were dried according to standard methods. Starting chemical substrates and reagents were used as commercially provided unless otherwise indicated. Thin layer chromatography (TLC) was performed on silica gel and the chromatograms were visualized using UV light (λ = 254 or 365 nm). Flash column chromatography was performed using silica gel (230-400 mesh). ^{1}H, ^{13}C and ^{11}B NMR spectra were recorded in $CDCl_3$ solution at 20 ºC. NMR chemical shifts are expressed in parts per million (δ scale). ^{1}H and ^{13}C NMR spectra are referenced to residual protons of $CDCl_3$ (δ = 7.26 and 77.16 ppm, respectively) as internal standard, ^{11}B spectra are referenced to 15% $BF_3 \cdot Et_2O$ in $CDCl_3$ (δ = 0.00 ppm) as external standard. The type of carbon (C, CH, CH_2 or CH_3) was assigned by DEPT-135 NMR experiments. Additionally, complex spin-system signals were simulated by using MestReNova program version 10.0.1-14719. FTIR spectra were obtained from neat samples using the attenuated total reflection (ATR) technique. High-resolution mass spectrometry (HRMS) was performed by using electrospray ionization (ESI) and hybrid quadrupole time-of-flight mass analyser (QTOF; positive-ion mode).

Photophysical properties

Spectroscopic signatures were recorded using diluted dye solutions (around 10^{-6} M) prepared from a concentrated stock solution in chloroform (around 10^{-3} M), after solvent evaporation under reduced pressure, and subsequent dilution with the desired solvent of spectroscopic grade, UV-vis absorption and fluorescence spectra were recorded on a Varian (model CARY 4E) spectrophotometer and an Edinburgh Instrument spectrofluorimeter (model FLSP 920), respectively. Fluorescence quantum yields (ϕ) were determined from corrected spectra (detector sensibility to the wavelength) by the optically dilute relative method. PM546 and PM567 (ϕ = 0.85 and 0.84, respectively, in ethanol) and cresyl violet (ϕ = 0.54 in methanol) were used as references.

The aforementioned spectrofluorimeter is also equipped with a wavelength-tunable pulsed Fianium laser. Thus, the Time Correlated Single-Photon Counting (TCSPC) technique was used to record the fluorescence decay curves. Fluorescence emission was monitored at the maximum emission wavelength after excitation by the said Fianium at the maximum absorption wavelength. The fluorescence lifetime (τ) was obtained from the slope of the exponential fit of the decay curve, after the deconvolution of the instrumental response signal (recorded by means of a ludox scattering suspension) by means of an iterative method. The goodness of the exponential fit was controlled by statistical parameters (chi-square and the analysis of the residuals).

Electrochemical properties

Redox potentials were measured by cyclic voltammetry (Metrohm Autolab) using a three-electrode set up with a platinum layer (surface 8 mm × 7.5 mm) working electrode, platinum wire as counter electrode, and Ag/AgCl as reference electrode. A 0.1 M solution of tetrabutylammonium hexafluorophosphate ($TBAPF_6$) in dry acetonitrile was used as the electrolyte solvent in which the compounds were dissolved to achieve a concentration of 0.5-1 mM. All redox potentials were reported vs ferrocene as internal standard. The solutions were purged with argon and all the measurements were performed under an inert atmosphere.

Delayed spectroscopy

Aerated solutions at room temperature of the dyes contained in 1-cm optical-path rectangular quartz cells were transversally pumped with intense laser pulses from the second and third harmonic (532 nm and 355 nm) of a Nd:YAG laser (LOTIS TII, LS-2147) at 10 Hz repetition rate. The time-gated emission upon laser photo-excitation, analyzed perpendicularly to the input radiation, was focused onto a spectrograph (Kymera 193i-A, Andor Technologies) coupled to an intensified CCD camera (iStar, Andor Technologies). This camera enables gate widths ranging from nanoseconds up to seconds, and its opening can be delayed in a controlled way with respect to the incoming pump laser pulse. Neither long-pass filters nor band-pass filters were used to remove the excitation laser since we have verified that these filters, especially long-pass ones, under drastic pump conditions, exhibited its own fluorescence and/or phosphorescence emission, which could lead to misunderstand the experimental results. Each spectrum is the average of at least 200 scans recorded with a gate time of 50 μs. The experiments were usually carried out at excitation energy fluence of 5 mJ/cm^2, which was varied from 1 up to 25 mJ/cm^2 to determine the dependence of the delayed fluorescence on the laser fluence. A solution volume of 3 cm^3 was used in order to avoid (or at least, to reduce) the risk of photo-bleaching the sample during the experiments. This experimental set-up allowed to carry out the projected measurements even under adverse conditions, but avoided to determine properly the efficiency of the delayed emission.

Quantum mechanics calculations

Ground state geometries were optimized within the Density Functional Theory (DFT), using different functionals as explained later on, and the triple valence basis set with a polarization function (6-311G*). In the compound bearing iodine atoms (**3**), the LANL2DZ basis set was used because the aforementioned basis set is not parameterized for such halogen. The geometries were considered as energy minimum when the corresponding frequency analysis did not give any negative value. From these optimized geometries, vertical electronic transition energies were calculated with the Time Dependent method (TD), since it is suitable for large molecules, with a reasonable balance between computational demand and calculation time.

The same method (TD-DFT) was used for the optimization of the first singlet excited state when available owing to the large molecular size of the MMAs and the ensuing unaffordable computational cost.

To check the accuracy of the selected functional in the DFT approach, we choose the unsubstituted boron-dipyrromethene (BDP) as a computationally more accessible model and studied in detail in the bibliography. The results provided by TD-B3LYP are far away from those reported with more advanced calculations like CASSCF and CASPT2 [1], especially in the S_1 state (around 0.6 eV), which is greatly overestimated as expected in view of the bibliographic precedents [2,3]. Such excited-state calculations methods are computationally unaffordable owing to the molecular size of the tested BODIPY-pyrene based MMAs. To ameliorate the results of TD-DFT we conducted a systematic analysis of the influence of the functional (range-separated hybrid functional WB97XD or the hybrid exchange-correlation functional CAM-B3LYP) [4,5] in the energy of the electronic levels of BDP. With regard to the CAS-based method, CAM-B3LYP yielded the best results (deviations <0.2 eV, [1] for the high-lying singlet and triplet states), but it still fails in the description of the absolute energies of the S_1 state (overestimated) as well of the associated T_1 state (underestimated by the same order of magnitude). This is why on the basis of the CASPT2 reported results for the BDP [1], we calculated a correction factor for the S_1 and T_1 states predicted by CAM-B3LYP. This is a common approach to get more realistic energy values for the prediction of absorption transitions with TD-DFT methods [6,7]. Such empirical correction implies a lowering of the S_1 state and, alternatively, an increase of the T_1 state (± 0.55 eV). To check the validity of the correction, we extrapolate the TD-DFT calculations to the rest of commercial BODIPYs available from Exciton. After applying such corrections, the ordering of the electronic levels is the expected one placing the T_2 above the S_1, being this the theoretically predicted funnel allowing the ISC in the bibliography [1]. Moreover, the predicted energy gaps for the S_1 state after correction accurately match those experimentally recorded from absorption spectra in solution (error lower than 0.02 eV, Figure S15). With regard to T_1 state, we compare its energy with that reported from phosphorescence spectra of common BODIPYs (around 1.7 eV). The predicted values are higher than the experimental ones, but this is logical since phosphorescence occurs from the relaxed T_1 state, which implies an energy lowering of around 0.1-0.2 eV [8]. Therefore, the empirical correction of TD-DFT is a suitable strategy to reproduce the substituent induced changes, such as spectral shift and arrangement of the energy levels.

We also considered the solvent effect in the calculations (PCM model) but the change in the energy of the electronic levels was quite low (less than 0.05 eV), as expected owing to the low solvatochromism of the spectral bands of BODIPYs in general, and of these MMAs in particular. So for the sake of simplicity, the herein reported results are in the gas phase.

All the theoretical calculations were carried out using the GAUSSIAN 16 program suite [9], implemented in the computational cluster provided by the SGIker resources of UPV-EHU.

Molecular dynamics

The initial configurations of the dye molecules **1** and **4** were relaxed using density functional theory (DFT) simulations implemented in Gaussian [9] with a B3LYP exchange-correlation functional [10] and the 6-311G* basis set, as shown in Figure S8. Two optimized dye molecules were placed randomly in a simulation box with dimensions 30Å×30Å×30Å and saturated with ethanol using Packmol [11]. The molecular dynamics simulations were carried out using the LAMMPS simulation package (29 Oct 2020 version) [12] in the computational cluster provided by the SGIker resources of UPV/EHU. The model was relaxed by performing an energy minimization and further equilibration in the isobaric−isothermal (NPT) ensemble at 1 atm and 300K using the reactive force field ReaxFF [13]. A Verlet integration scheme [14] with a time step of 1 fs and a Noose-Hoover thermostat and barostat with coupling constants of 0.1 ps and 1 ps were applied. After the initial equilibration, a MD trajectory is recorded for production for 5 ns in the canonical (NVT) ensemble at 300K. All figures are prepared using TRAVIS [15], Mathematica [16] and VESTA [17].

2. Synthetic procedures and characterization data

Synthesis of MMAs 1 and 2

COO-BODIPY-based MMA **1** and **2** were obtained from the corresponding *F*-BODIPY and pyrene-1-carboxylic acid (see Scheme 1) as reported recently by us [18].

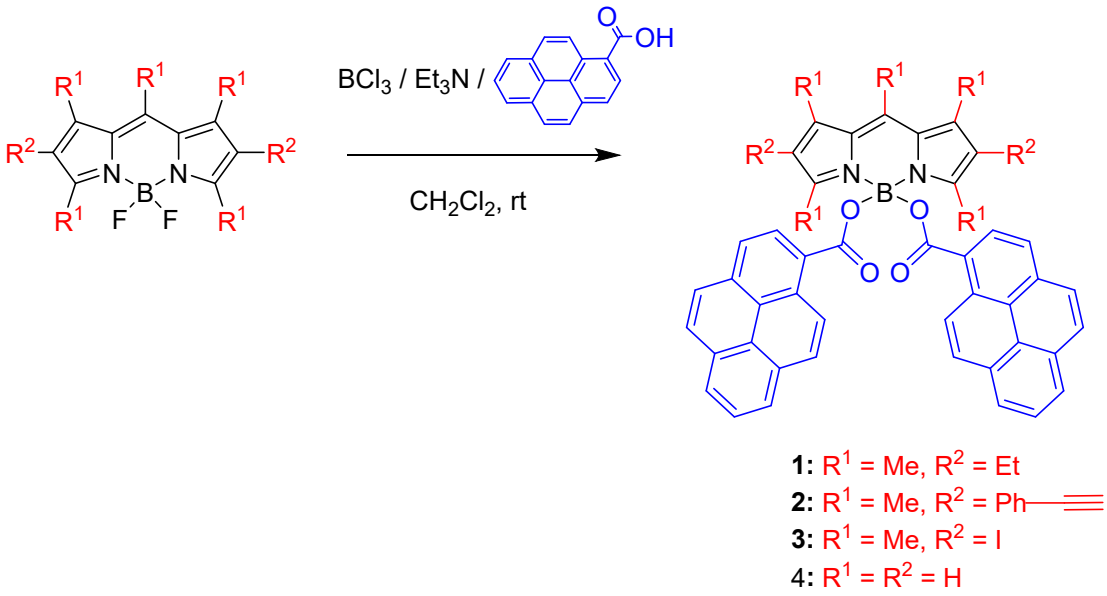

Scheme S1. General synthetic outline.

Synthesis of MMAs 3 and 4

Synthesis of *F*-BODIPY precursors: Simplest (non-substituted) *F*-BODIPY (4,4-difluoroBODIPY) was synthesized from commercial pyrrole and paraformaldehyde according to the procedure reported by Thompson *et al*. [19], whereas 2,6-diiodo-1,3,5,7,8-pentamethyl-*F*-BODIPY was obtained by electrophilic iodination of 1,3,5,7,8-pentamethyl-*F*-BODIPY (PM546) with *N*-iodosuccinimide according to the synthetic procedure reported by Koivisto *et al.* [20].

MMA 3: BCl_3 (1 M in CH_2Cl_2; 0.18 mL, 0.18 mmol) was dropwise added over a solution of 2,6-diiodo-1,3,5,7,8-pentamethyl-*F*-BODIPY (46 mg, 0.09 mmol) in dry CH_2Cl_2 (5 mL) under argon atmosphere. The mixture was stirred at room temperature for 5 min. Then, triethylamine (0.075 mL, 0.54 mmol) was added over the solution, followed by addition of pyrene-1-carboxylic acid (86 mg, 0.35 mmol), and the resulting mixture was stirred for further 30 min (the reaction evolution was monitored by TLC). Once the reaction was completed, the reaction mixture was filtered through Celite® S, and the celite washed thoroughly with CH_2Cl_2. The filtered solution was submitted to solvent evaporation under reduced pressure, and the obtained residue to purification by flash chromatography (silica gel, hexane/ CH_2Cl_2 4:6) to obtain **3** (67 mg, 77%) as a red solid. R_F = 0.26 (hexane/CH_2Cl_2 4:6). ^{1}H NMR ($CDCl_3$, 500 MHz) δ 9.45 (d, J = 9.5 Hz, 2H), 8.97

(d, J = 8.1 Hz, 2H), 8.27 (d, J = 7.8 Hz, 4H), 8.26 (d, J = 8.1 Hz, 2H), 8.22 (d, J = 9.4 Hz, 2H), 8.20 (d, J = 8.9 Hz, 2H), 8.13 (d, J = 8.8 Hz, 2H), 8.06 (t, J = 7.6 Hz, 2H), 2.87 (s, 3H), 2.68 (s, 6H), 2.59 (s, 6H) ppm. ^{13}C NMR ($CDCl_3$, 176 MHz) δ 167.6 (C), 153.4 (C), 143.3 (C), 142.3 (C), 134.4 (C), 134.0 (C), 131.6 (C), 131.2 (C), 130.5 (C), 129.7 (CH), 129.4 (CH), 129.3 (CH), 127.4 (CH), 126.4 (CH), 126.3 (CH), 126.2 (CH), 125.6 (CH), 125.3 (C), 125.2 (C), 124.5 (C), 124.4 (CH), 86.6 (C), 20.5 (CH_3), 18.7 (CH_3), 16.8 (CH_3) ppm. ^{11}B NMR ($CDCl_3$, 160 MHz) δ 0.56 ppm. FTIR ν 1693, 1542, 1523, 1253, 1189, 1135, 995 cm^{-1}. HRMS (ESI$^+$/Q-TOF) *m/z* 989.0499 ([M+Na]$^+$; Calcd for $C_{48}H_{33}BI_2N_2O_4Na$, 989.0520).

MMA 4: According to the procedure described for MMA **3**, 4,4-difluoroBODIPY (24 mg, 0.13 mmol) was reacted with pyrene-1-carboxylic acid (121 mg, 0.49 mmol) upon treatment with BCl_3 (1 M in CH_2Cl_2; 0.25 mL, 0.25 mmol) and Et_3N (1.10 mL, 0.79 mmol). After filtration through celite and solvent evaporation, the obtained residue was purified by flash chromatography (silica gel, CH_2Cl_2) to obtain **4** (37 mg, 46%) as a yellowish orange solid. R_F = 0.36 (hexane/CH_2Cl_2 4:6). ^{1}H NMR ($CDCl_3$, 500 MHz) δ 9.44 (d, J = 9.4 Hz, 2H), 8.91 (d, J = 8.1 Hz, 2H), 8.43 (br s, 2H), 8.24 (d, J = 7.6 Hz, 2H), 8.24 (d, J = 7.4 Hz, 2H), 8.21 (d, J = 8.1 Hz, 2H), 8.19 (d, J = 9.5 Hz, 2H), 8.17 (d, J = 8.9 Hz, 2H), 8.10 (d, J = 8.9 Hz, 2H), 8.04 (t, J = 7.6 Hz, 2H), 7.73 (br s, 1H), 7.34 (d, J = 4.2 Hz, 2H), 6.64 (dd, J = 4.3, 1.9 Hz, 2H) ppm. ^{13}C NMR ($CDCl_3$, 75 MHz) δ 168.4 (C), 146.5 (CH), 136.3 (C), 134.2 (C), 131.9 (CH), 131.5 (CH), 131.4 (C), 131.2 (C), 130.6 (C), 129.4 (CH), 129.1 (CH), 127.4 (CH), 126.3 (CH), 126.1 (CH), 126.1 (CH), 125.7 (CH), 125.1 (C), 124.5 (C), 124.4 (CH), 119.1 (CH), 119.09 (C) ppm. ^{11}B NMR ($CDCl_3$, 160 MHz) δ 0.69 (s) ppm. FTIR ν 1670, 1593, 1402, 1288, 1047 cm^{-1}. HRMS (ESI$^+$/Q-TOF) *m/z* 667.1833 ([M+Na]$^+$ Calcd for $C_{43}H_{25}BN_2O_4Na$, 667.1812).

3. ^{1}H, ^{13}C, and ^{11}B NMR spectra of new compounds

^{1}H NMR ($CDCl_3$, 500 MHz) of 3

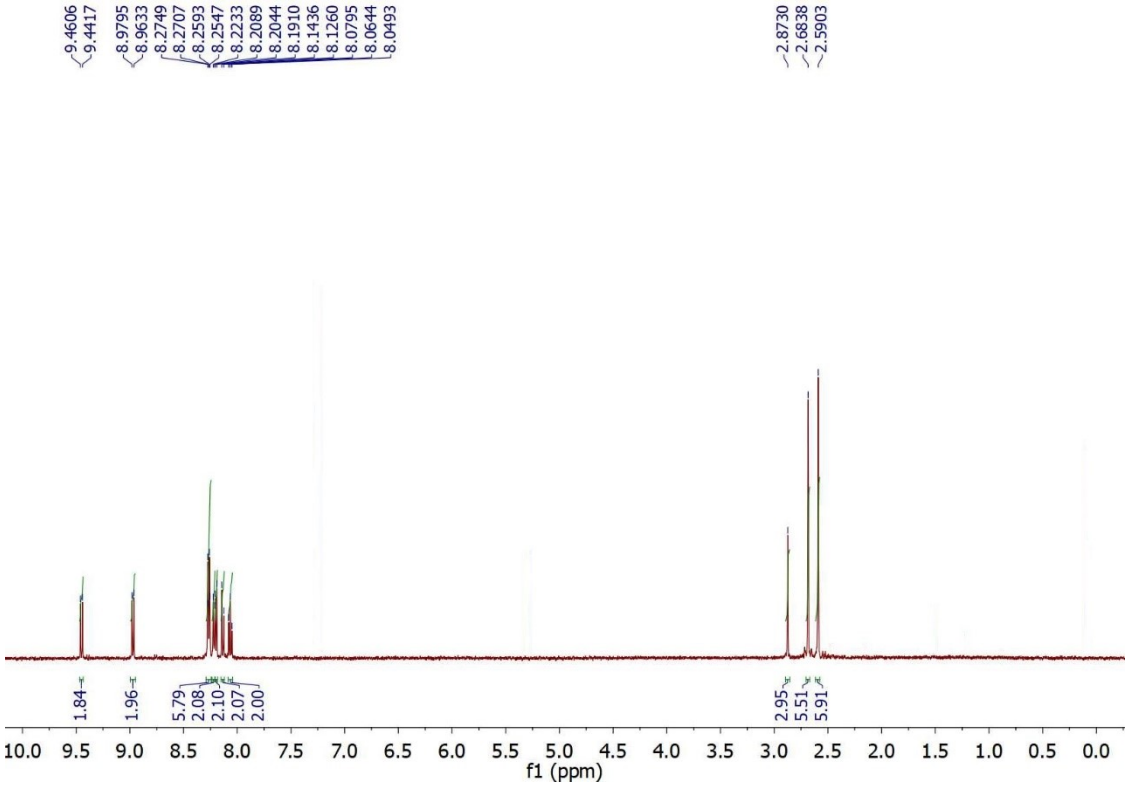

^{13}C NMR ($CDCl_3$, 176 MHz) of 3

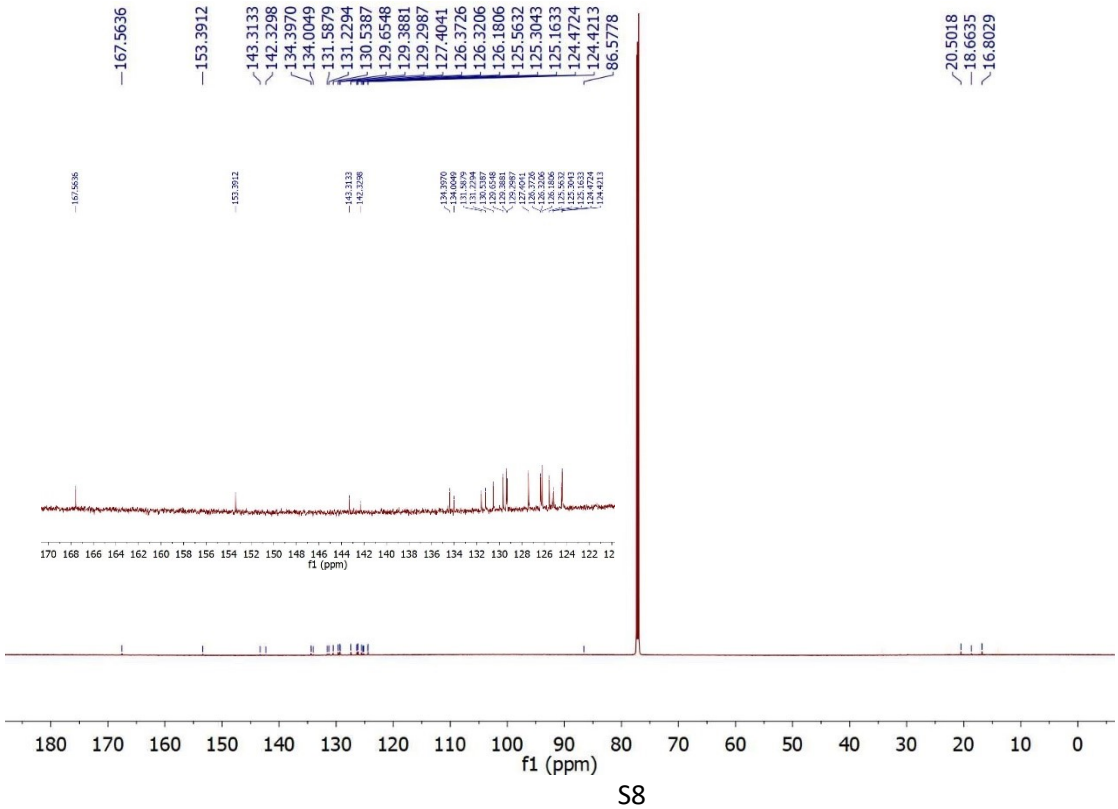

^{11}B NMR ($CDCl_3$, 160 MHz) of 3

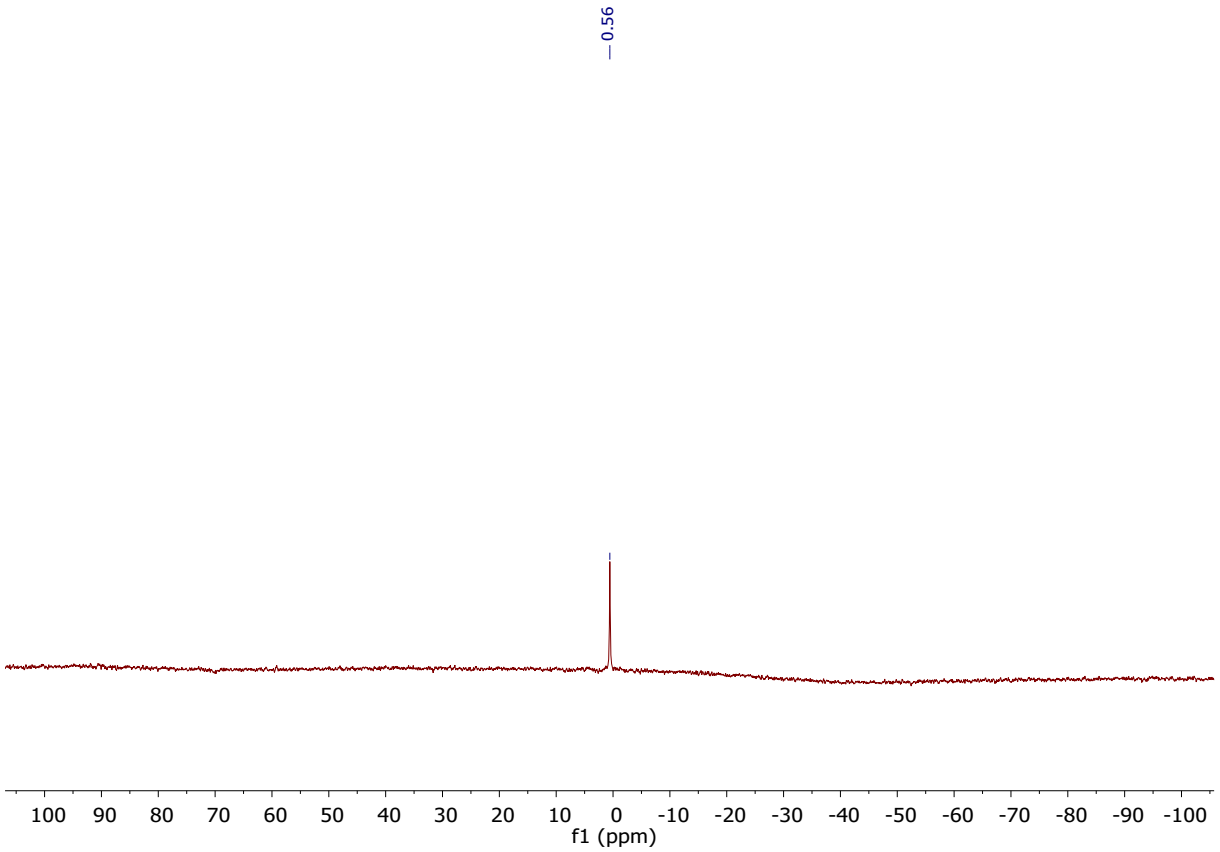

^{1}H NMR ($CDCl_3$, 500 MHz) of 4

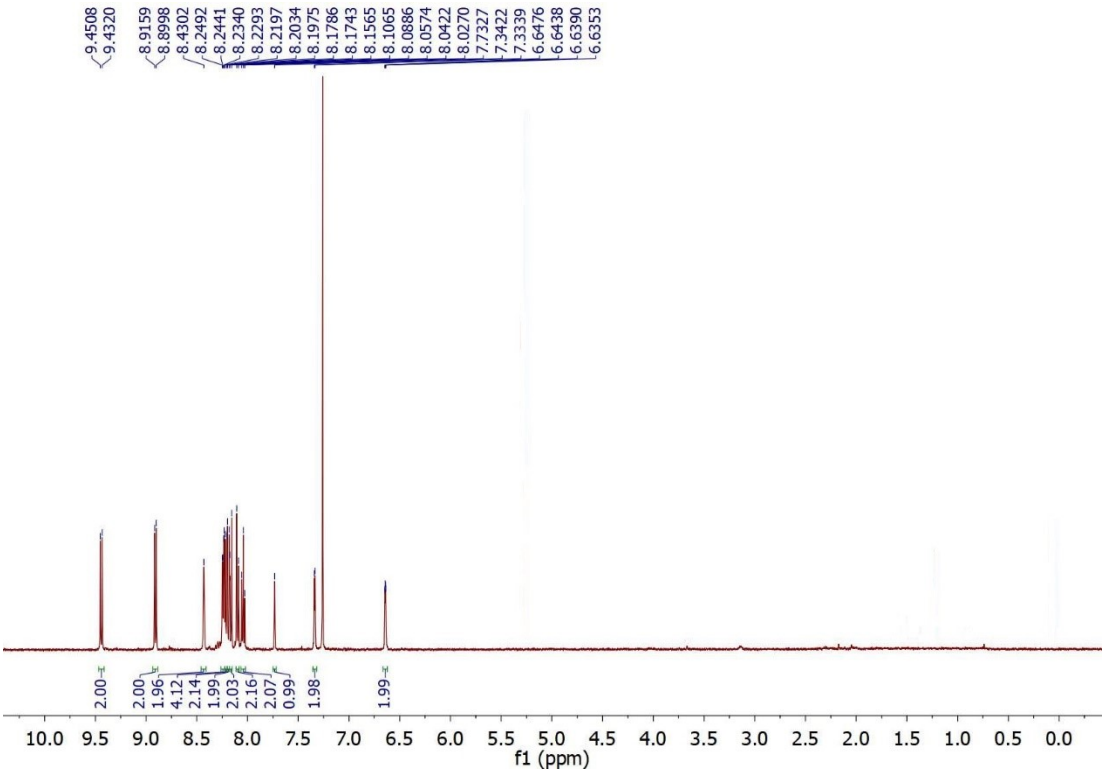

^{13}C NMR ($CDCl_3$, 75 MHz) of 4

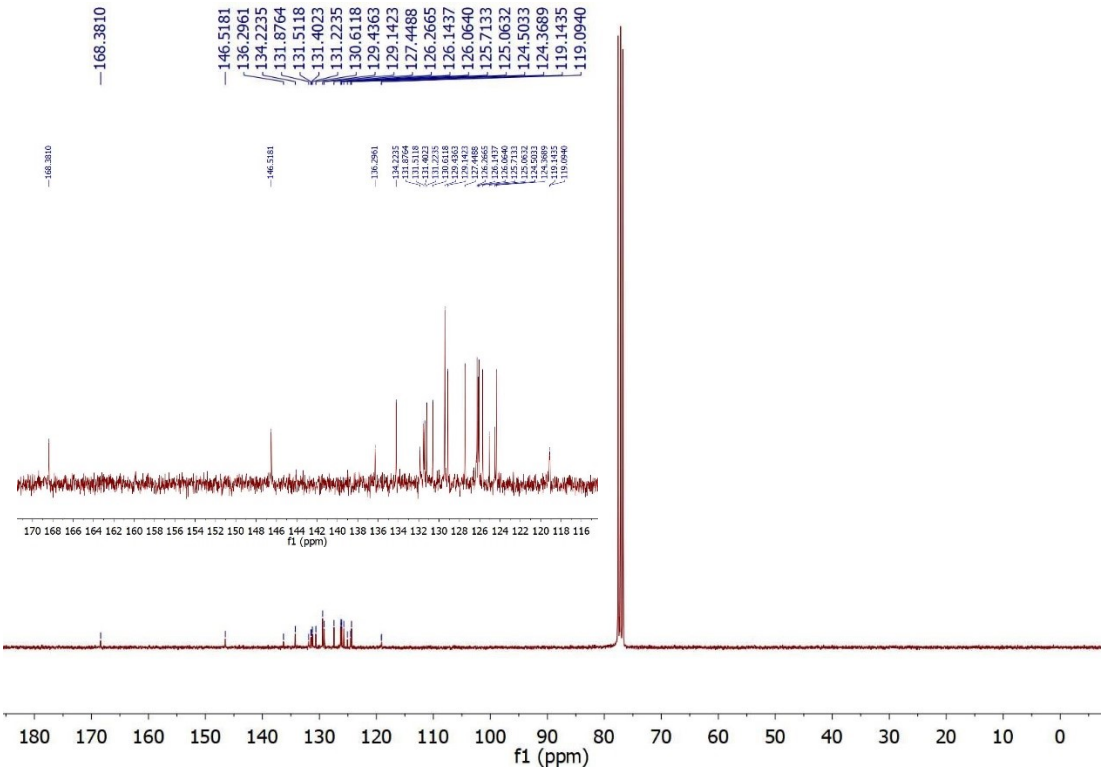

^{11}B NMR ($CDCl_3$, 160 MHz) of 4

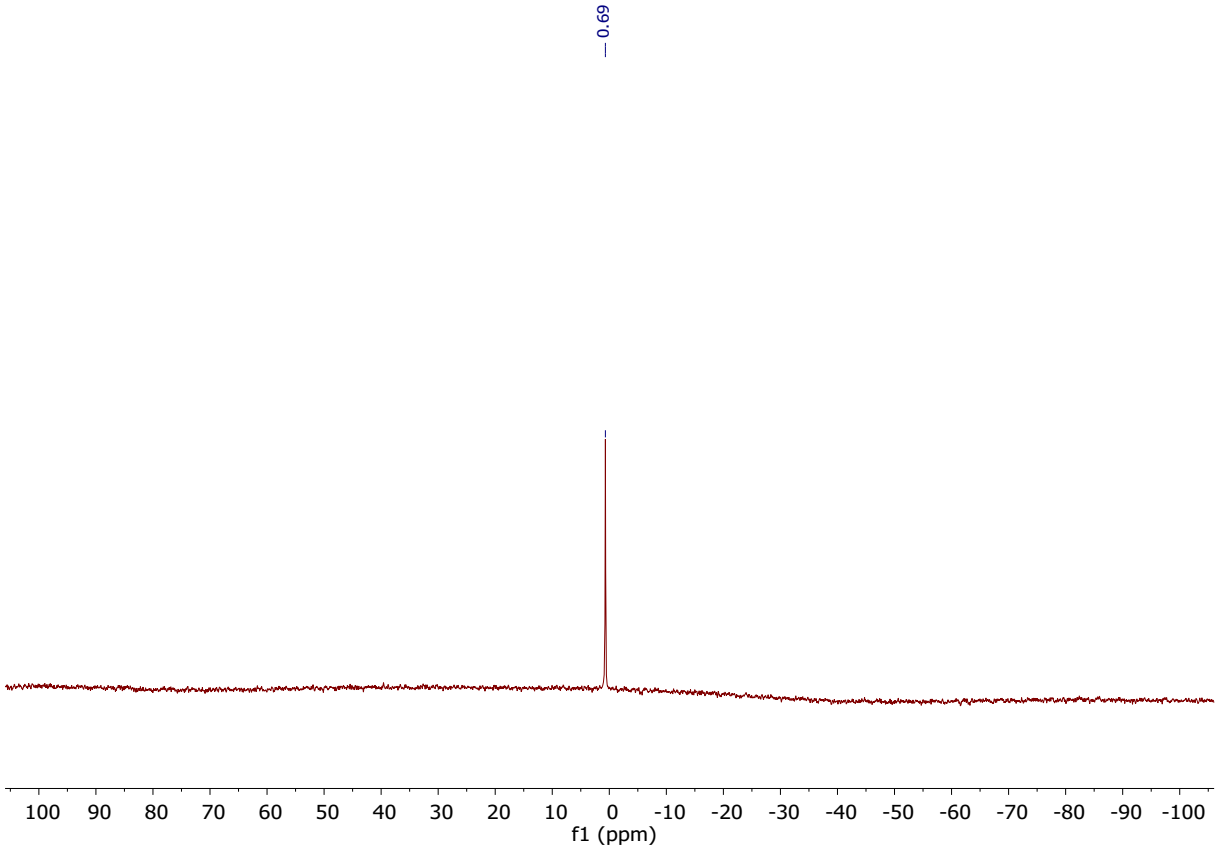

4. Photophysical and lasing properties

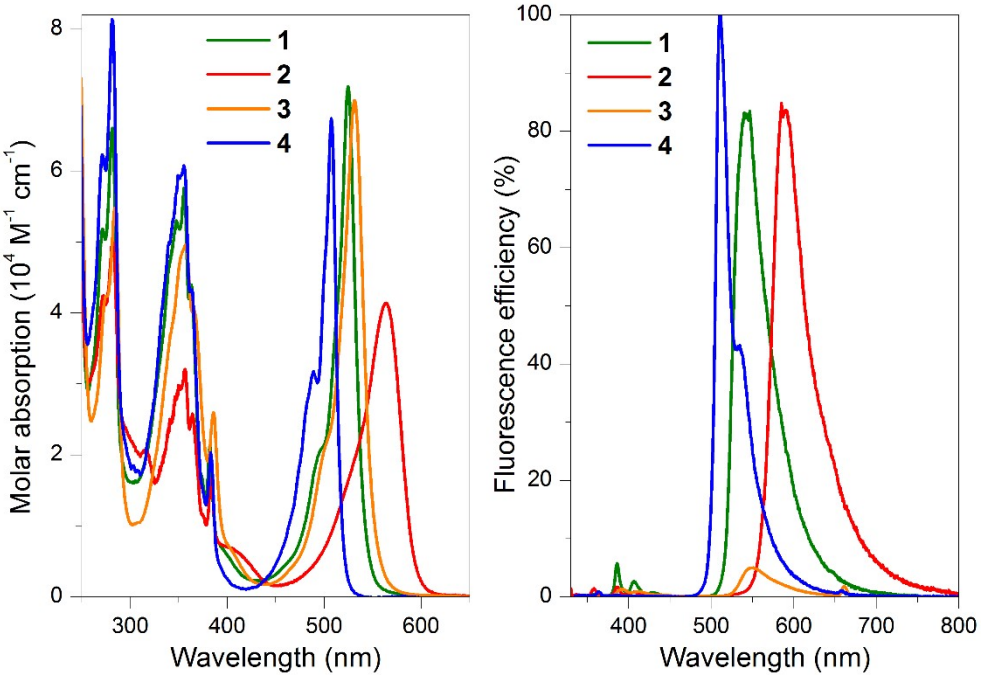

Figure S1. Absorption and fluorescence (after selective excitation of the pyrene at 330 nm) of the BODIPY/pyrene PTT-MMAs **1-4** in diluted solutions of cyclohexane.

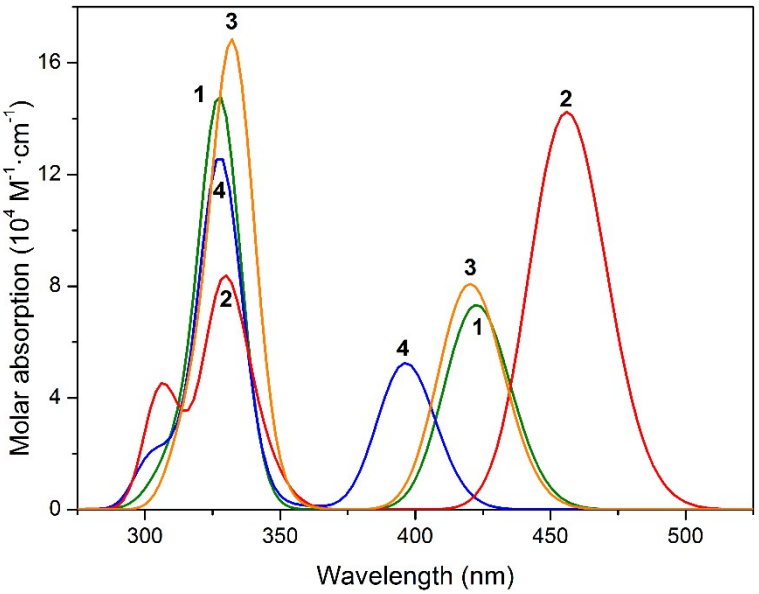

Figure S2. Theoretically predicted (CAM-B3LYP) absorption spectra of the BODIPY/pyrene PTT-MMAs **1-4**. The basis set was 6-311 G*, except for the iodine bearing compound where LANL2DZ was used.

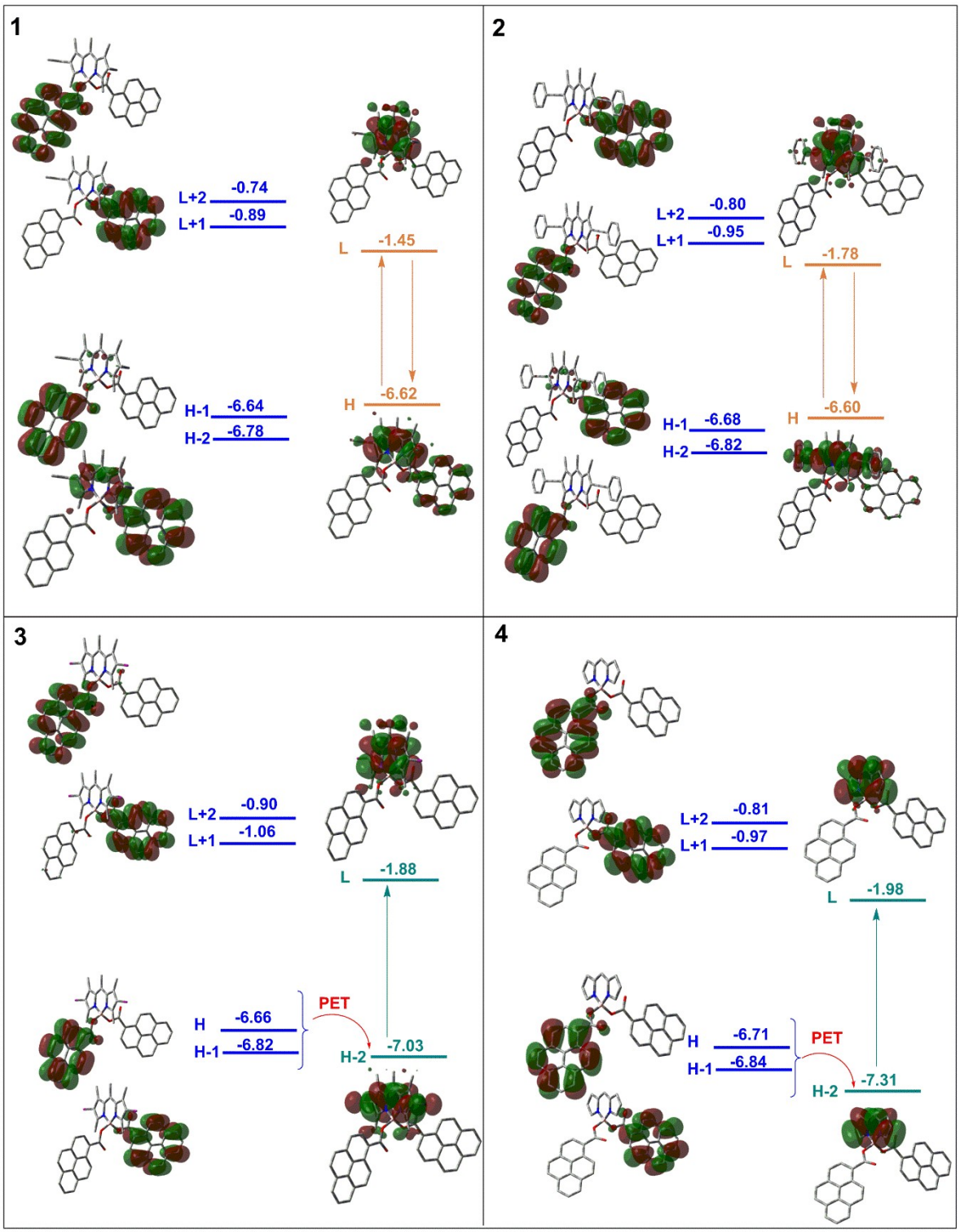

Figure S3. Calculated (B3LYP/6-311G*) electronic density and energies (in eV) of the molecular orbitals involved in the main electronic transitions of BODIPY/pyrene MMAs **1-4**.

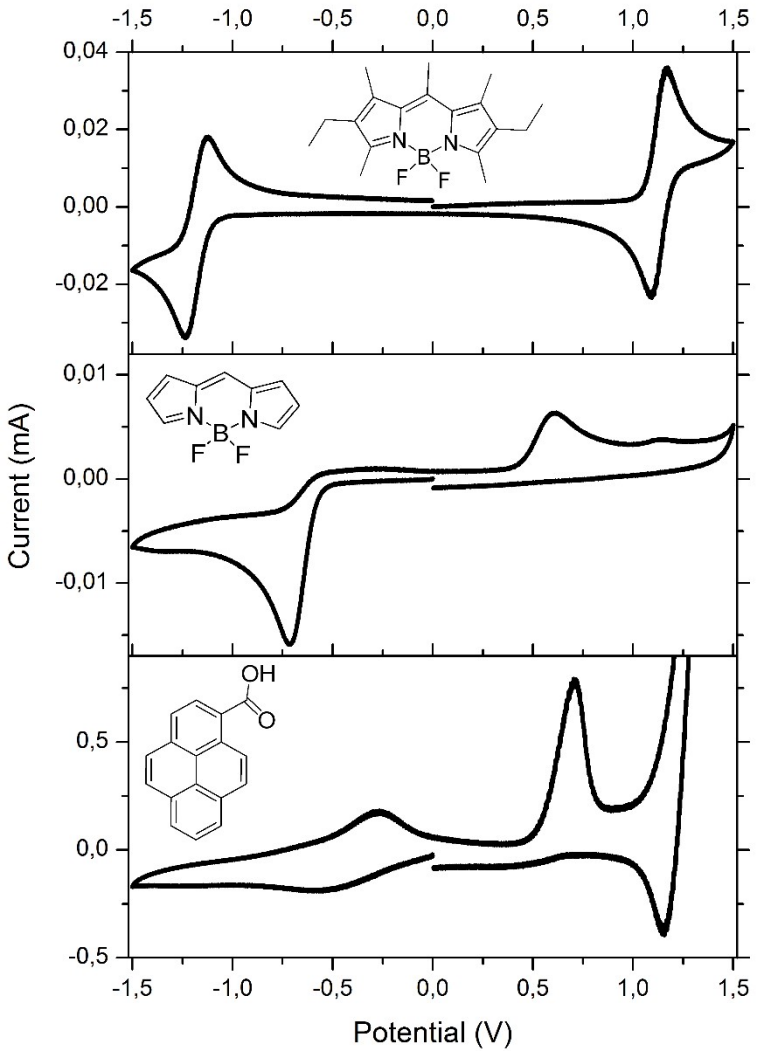

Figure S4. Cyclic voltammograms of the chromophoric subunits (corresponding dye precursors) involved in BODIPY/pyrene PTT-MMAs **1** and **4** (disabling and enabling PET, respectively).

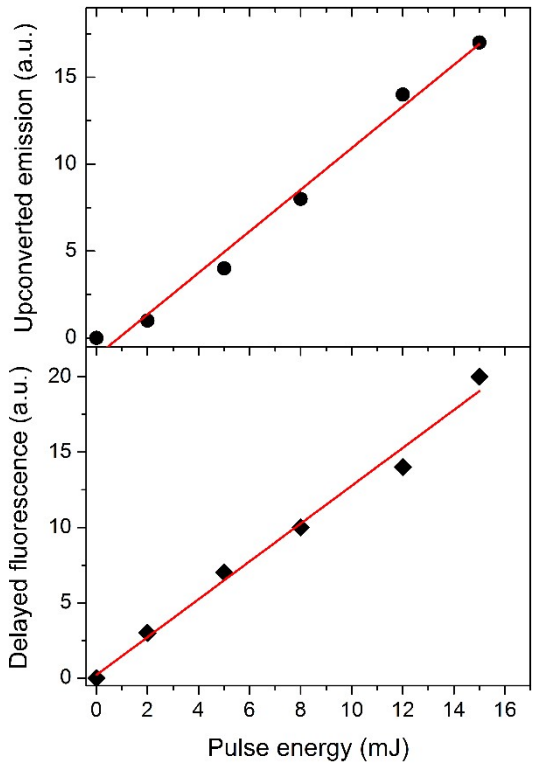

Figure S5. Delayed fluorescence intensity from BODIPY/pyrene PTT-MMA **1** (5×10^{-5} M), after selective excitation of the BODIPY subunit at 532 nm and recording emission at longer wavelengths (bottom), and TTA-UC emission intensity from BODIPY/pyrene PTT-MMA **2** (5×10^{-5} M), after same excitation wavelength but recording emission at shorter wavelengths (top), in aerated ethyl acetate, as a function of the laser excitation energy.

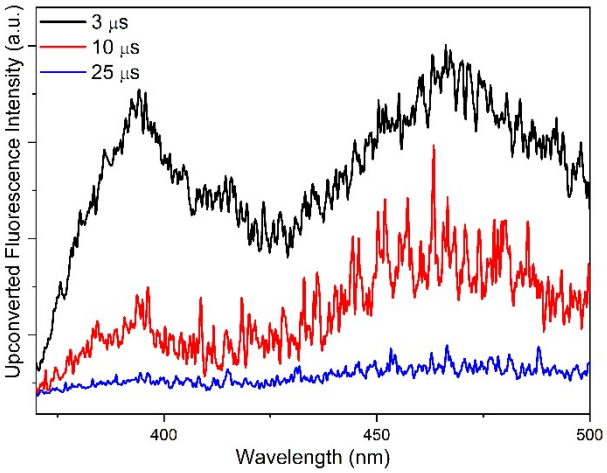

Figure S6. Time-dependent upconverted emission spectra from PTT-MMA **1** ($1\text{x}10^{-5}$ M) in aerated ethyl acetate solution at room temperature upon laser excitation at 532 nm and 12 mJ/pulse.

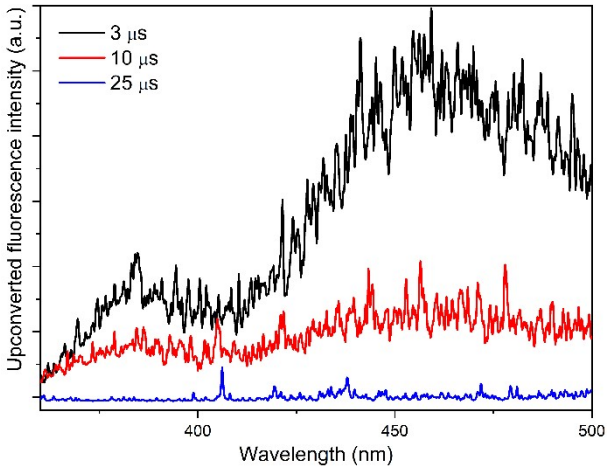

Figure S7. Time-dependent upconverted emission spectra from PTT-MMA **1** ($1x10^{-4}$ M) in aerated ethyl acetate solution at room temperature upon laser excitation at 532 nm and 2 mJ/pulse.

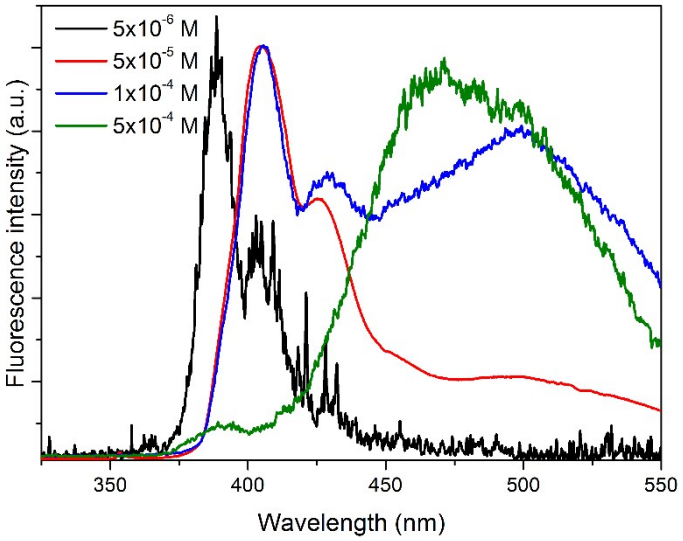

Figure S8. Concentration dependence of the prompt fluorescence spectra of pyrene-1-carboxylic acid alone in ethyl acetate after laser excitation at 355 nm. For comparison purposes, the spectra recorded from 5×10^{-6} M to 1×10^{-4} M were normalized to the monomer emission.

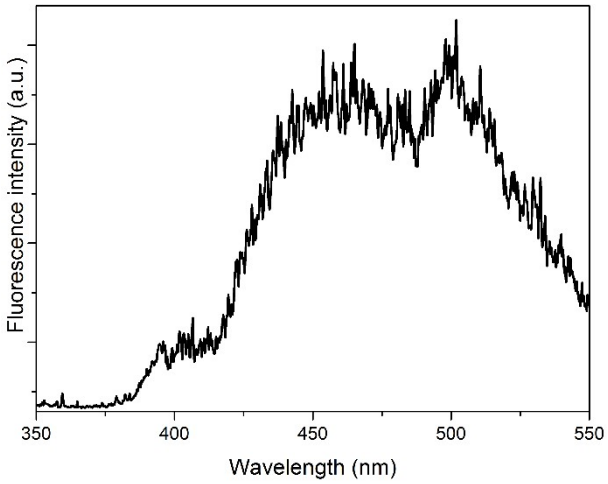

Figure S9. Upconverted emission from PM567 physically mixed with pyrene-1-carboxylic acid ([PM567] = 1×10^{-5} M and [pyrene-1-carboxylic acid] = 3×10^{-4} M) after laser excitation at 532 nm.

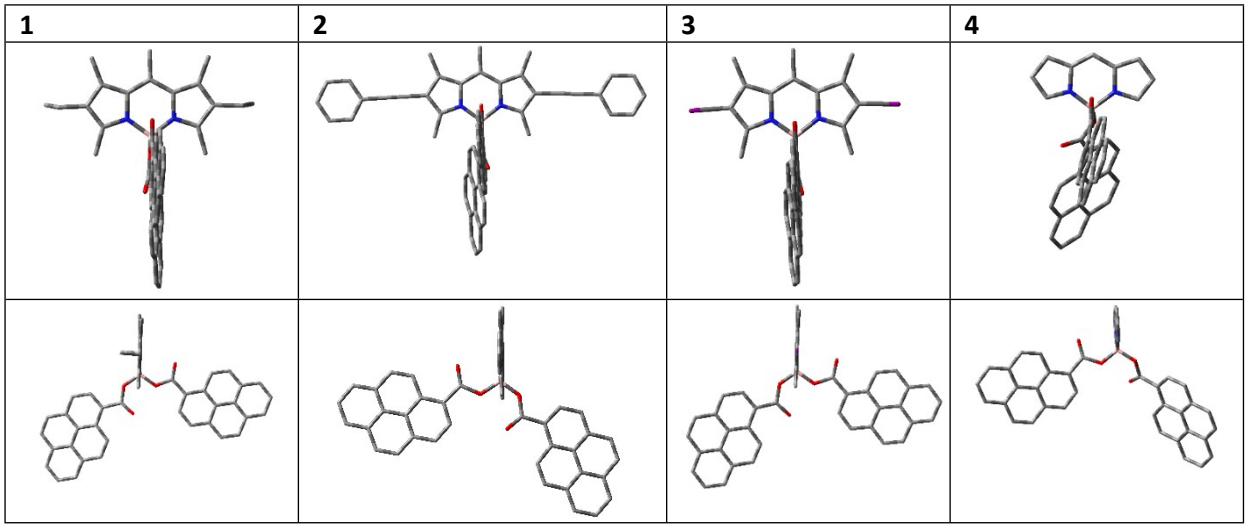

Figure S10. Optimized (B3LYP/6-311g*) ground state geometries of BODIPY/pyrene PTT-MMAs **1**-**4** in two different views to highlight the orthogonal arrangement of the pyrene moieties with respect to the BODIPY one, being the former chromophores disposed coplanar, but in opposite orientations.

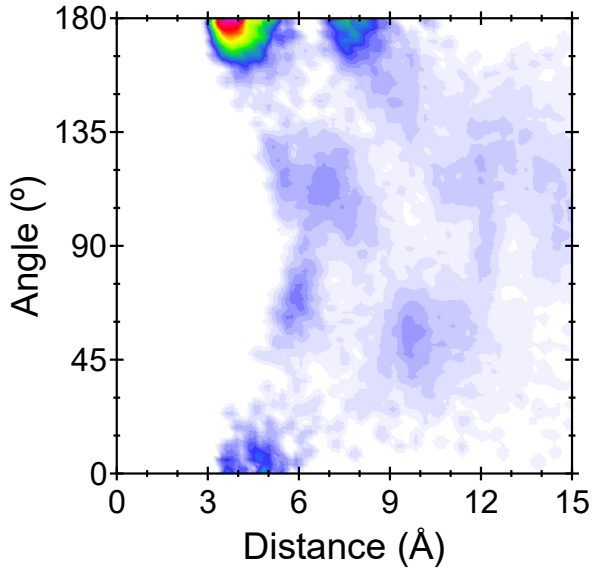

Figure S11. Combined distribution function of the dihedral angle formed by the plane of the pyrenes and the distance between their centers of masses in BODIPY/pyrene PTT-MMA **4**.

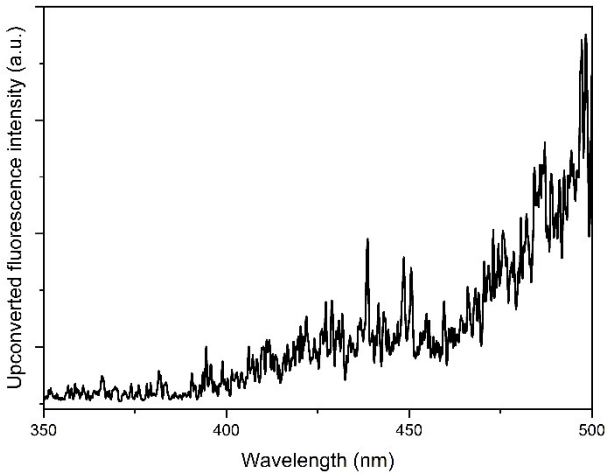

Figure S12. Upconverted emission spectrum upon laser excitation at 532 nm and 12 mJ/pulse from PTT-MMA **1** ($5x10^{-6}$ M) in aerated ethyl acetate solution at room temperature recorded at 3 μs after excitation.

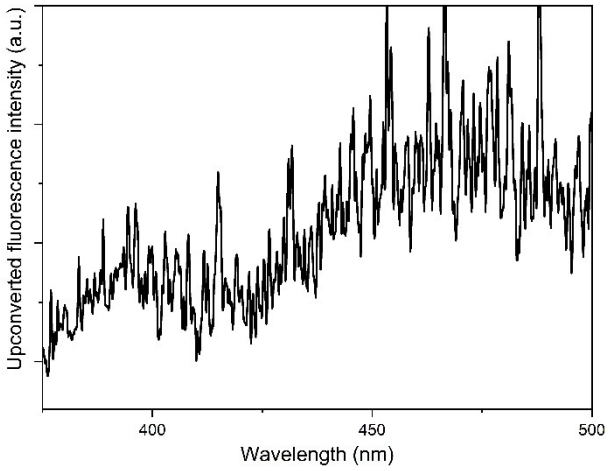

Figure S13. Upconverted emission spectrum upon laser excitation at 532 nm and 12 mJ/pulse from PTT-MMA **1** ($5x10^{-6}$ M) in ethylene glycol solution at room temperature recorded at 3 μs after excitation.

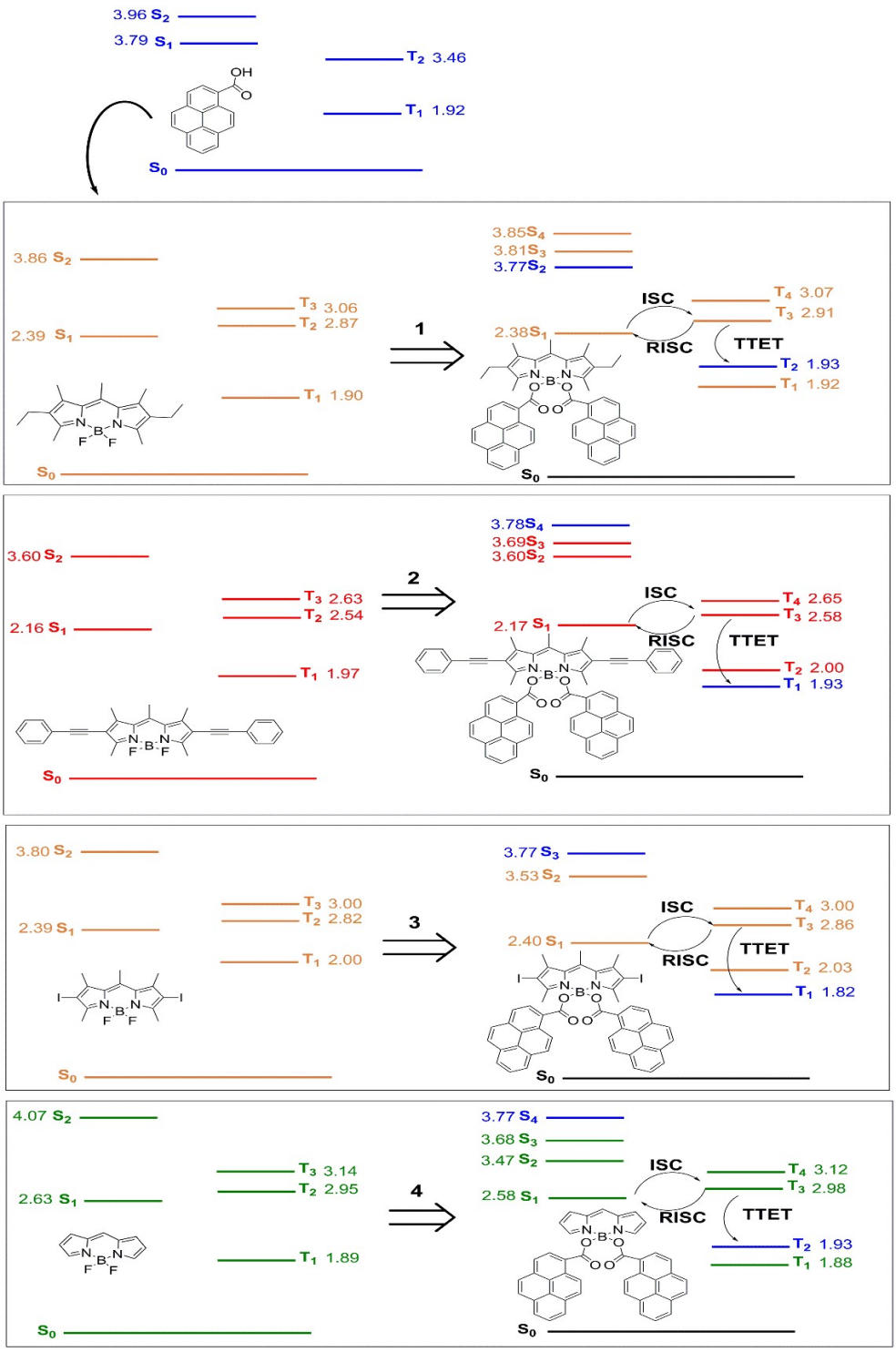

Figure S14. Schematic view of the calculated (CAM-B3LYP) energetic distribution of the singlet and triplet manifolds of the BODIPY/pyrene PTT-MMAs **1-4** and their respective isolated chromophoric subunits.

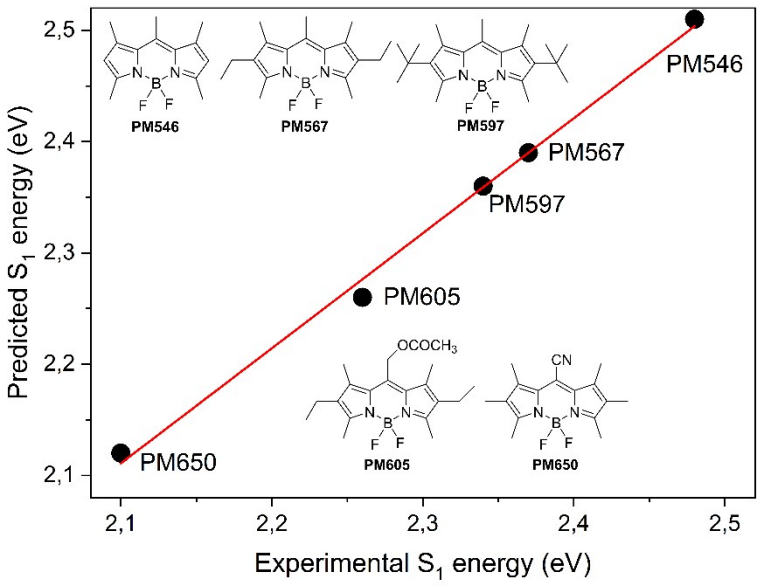

Figure S15. Correlation between the experimental absorption energies of commercially available BODIPYs (Exciton; data in cyclohexane), and the predicted one with the empirically corrected (reference CASPT2 in BDP [1]) CAM-B3LYP calculation in the gas phase.

5. References

[1] M. De Vetta, L. González and I. Corral, *ChemPhotoChem,* 2019, **3**, 727-738.

[2] M. R. Momeni and A. Brown, *J. Chem. Theory Comput,.* 2015, **11**, 2619-2632.

[3] P.-F. Loos, A. Scemana and D. Jacquemin, *J. Phys. Chem. Lett.,* 2020, **11**, 2374-2383.

[4] J. C. Howard, J. D. Enyard and G. S. Tschumper, *J. Chem. Phys.,* 2015, **143**, 214103.

[5] S. R. Jensen, S. Saha, J. A. Flores-Livas, W. Huhn, V. Blum, S. Goedecker and L. Frediani, *J. Phys. Chem. Lett.,* 2017, **8**, 1449-1457.

[6] A. Schlachter, A. Fleury, K. Tanner, A. Soldera, B. Habermeyer, R. Guilard and P. D. Harvey, *Molecules* 2021, **26**, 1780.

[7] J.-N. Wang, J.-L. Jin, Y. Geng, S.-L. Sun, H.-L. Xu, Y.-H. Lu and Z.-M. Su, *J. Comput. Chem.,* 2013, **34**, 566-575.

[8] M. Buyuktemiz, S. Duman and Y. Dede, *J. Phys. Chem. A,* 2013, **117**, 1665-1669.

[9] M. J. Frisch, G. W. Trucks, H. B. Schlegel, G. E. Scuseria, M. A. Robb, J. R. Cheeseman, G. Scalmani, V. P. G. A. Barone, G. A. Petersson, H. Nakatsuji & D. J. Fox, Gaussian 16, Gaussian, Inc.: Wallingford, CT, 2016.

[10] K. Kim and K. Jordan, *J. Phys. Chem.,* 1994, **98**, 10089−10094.

[11] L. Martínez, R. Andrade, E. G. Birgin and J. M. Martínez, *J. Comput. Chem.,* 2009, **30**, 2157-2164.

[12] A. P. Thompson, H. M. Aktulga, R. Berger, D. S. Bolintineanu, W. M. Brown, P. S. Crozier, P. J. in't Veld, A. Kohlmeyer, S. G. Moore and T. D. Nguyen, *Comput. Phys. Commun.,* 2022, **271**, 108171.

[13] M. M. Islam and A. C. T. Van Duin *J. Phys. Chem. C,* 2016, **120**, 27128-27134.

[14] H. Grubmüller, H. Heller, A. Windemuth and K. Schulten *Mol. Simul.,* 1991, **6**, 121-142.

[15] M. Brehm, M. Thomas, S. Gehrke and B. Kirchner, *J. Chem. Phys.,* 2020, **152**, 164105.

[16] Wolfram Research, Inc., Mathematica, Version 13.0.0, Champaign, IL, 2021.

[17] K. Momma and F. Izumi, *J. Appl. Crystallogr.,* 2011, **44**, 1272–1276.

[18] C. Ray, C. Schad, E. Avellanal-Zaballa, F. Moreno, B. L. Maroto, J. Bañuelos, I. García-Moreno and S. de la Moya, *Chem. Commun*., 2020, **56**, 13025-13028.

[19] B. R. Groves, S. M. Crawford, T. Lundrigan, C. F. Matta, S. Sowlati-Hashijin and A. Thompson, *Chem. Commun.,* 2013, **49**, 816-818.

[20] C. Bonnier, D. D. Machin, O. Abdi and B. D. Koivisto, *Org. Biomol. Chem.,* 2013, **11**, 3756-3760.